

SIGNIFICANCE:

Genome packaging in viruses – The Question: Viruses follow one of two basic strategies to package their chromosomes. In one, the viral capsid proteins interact with and polymerize around viral chromosomes. In the second, an empty procapsid is assembled, and then a virally encoded motor pumps the viral genome into this preassembled container. The latter strategy is used by most double-stranded DNA bacteriophages and their eukaryotic counterparts, the herpes-, adeno-, and poxviruses^{1,2}. Here we will determine, in atomic detail, how viral DNA packaging machines convert ATP binding, hydrolysis, and release into mechanical force.

ASCE ring ATPase motors – The Broader Impact: The molecular motors that power viral dsDNA translocation are members of an ancient and widely distributed class of ATPase ring motors, the additional strand conserved glutamate (ASCE) ATPases³. ASCE motors participate in a wide range of cellular functions involving moving and/or manipulating biological polymers, including during DNA replication, chromosome segregation, and protein degradation⁴. In dsDNA viruses, the ASCE ATPase ring motor drives DNA through a unique vertex of the procapsid receptacle, overcoming the resistive forces of entropy, DNA-bending, and electrostatic repulsion of the highly charged DNA. Our single-molecule studies have shown that these motors can exert forces greater than 50pN and are thus among the most powerful known⁵. Our previous work shows that dsDNA packaging motors provide a clear view into the mechanochemistry of force-generation found in ASCE motors. As human innovation is often inspired by nature, understanding the mechano-chemistry utilized by these motors will likely inspire the rational design of synthetic molecular motors. Indeed, rationally modified helicase motors can perform all necessary strand separations in PCR, eliminating the need for thermocycling⁶.

Our hypothesis is that DNA packaging is driven by tightly regulated helical-to-planar transitions within the ATPase ring motor^{7–9}. Briefly, sequential ATP binding causes each subunit to bind the DNA phosphate backbone, distorting the planar ring motor into an all-ATP bound helical configuration, creating mechanical strain in the ring. Subsequent sequential hydrolysis events alleviate the accumulated strain, allowing a stepwise return of the motor to the planar conformation, thereby translocating DNA. Given the ubiquity of ASCE motors, the helical-to-planar mechanism could serve as a general framework for certain ring ATPases⁴.

φ29 as model systems for investigating dsDNA packaging: We use the phi29 (ϕ 29)-like phages as model systems to investigate DNA packaging motors^{2,10}. The packaging machinery (Fig. 1) assembles at a unique vertex of an icosahedral shell that is occupied by a dodecameric portal ring (connector). In addition to the portal and the ATPase ring, the ϕ 29 packaging machinery also includes an oligomeric RNA, prohead RNA (pRNA), that serves as a scaffold for assembly of a pentameric ATPase ring. After packaging, the pRNA and ATPase detach to allow attachment of a tail. A robust *in vitro* DNA packaging system for ϕ 29 has been developed wherein purified procapsids and ATPase can be package DNA with over 80% efficiency¹⁰. Owing to the accessible nature of this packaging system, it has been possible to interrogate the packaging process using a wide range of experimental tools, including genetic, biochemical, biophysical, structural, and single-molecule approaches.

Single-molecule advances: Single-molecule analysis showed that the ϕ 29 packaging motor operates in a highly coordinated manner (Fig. 2)^{11–13}. Our early work indicated that the mechanochemical cycle of the motor is separated into two distinct phases. During the “dwell” phase, all five ATPase subunits release ADP and load ATP in a sequential, interlaced manner – DNA is not translocated during these steps. During the subsequent “burst” phase, the motor sequentially hydrolyzes ATP, driving 10 bp of dsDNA into the procapsid. Later higher resolution laser tweezers experiments showed that each 10-bp burst consisted of 4 x 2.5 base-pair steps, raising the question of how a 5-subunit motor takes only 4 steps.

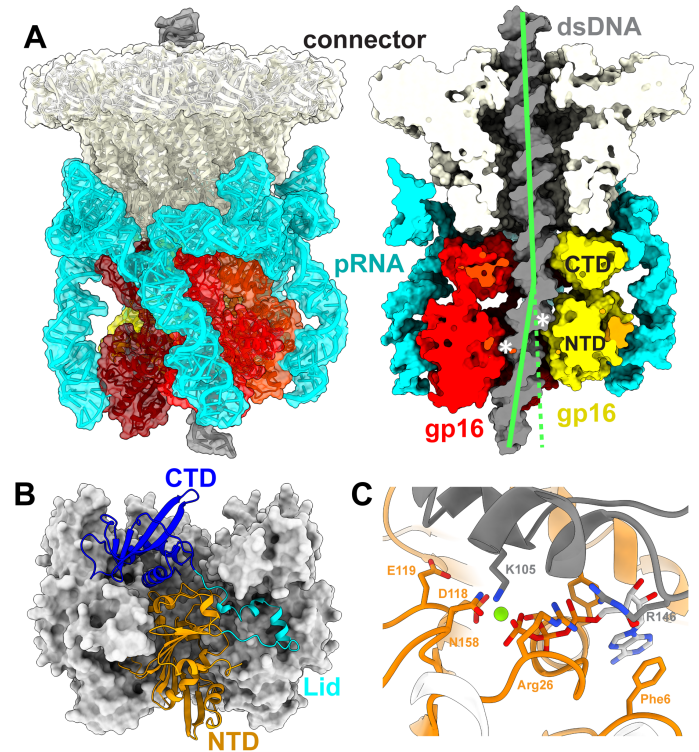


Fig. 1: (A) Left: Structure of the ϕ 29 packaging motor. Right: The helical rise of subunits (* indicate equivalent NTD-DNA contacts), and the kink of DNA (green line). (B) Structure of the planar ascc ϕ 28 pentamer; one subunit depicted as ribbons and colored by domain. Other subunits are shown as space-filling depictions. (C) ϕ 29 motor active site: trans-acting residues in gray, and the cis-acting residues as orange.

Similarly, translocating DNA in non-integer bp steps is puzzling, as it would seem analogous to climbing a ladder a non-integer number of rungs at a time.

We have also shown that DNA rotates 14° during each 10-bp translocation burst to maintain motor/DNA alignment since DNA has a periodicity of 10.4 base pairs per helical turn¹³. It was not clear if DNA rotation occurs in one 14° step, or if the rotation is distributed over smaller steps that accompany each 2.5 bp translation. To reconcile a 5-subunit motor taking only 4 steps, hydrolysis in the 5th subunit was proposed to play a regulatory role and was generally believed to initiate the burst.

Structural advances: Whereas our extensive single-molecule analysis provided a detailed scheme of what happens during packaging (Fig. 2), the physical basis of force generation and subunit coordination remained largely unknown. Hence, we have used various structural approaches to characterize the motor. We determined the first atomic resolution structures of a viral portal protein¹⁴, the pRNA^{15,16}, and both the N-terminal ASCE domain¹⁷ (NTD) and the C-terminal domain¹⁸ (CTD) of the φ29 packaging ATPase. To fit structures into cryoEM maps, we pioneered the use of ‘difference images’ and focused reconstruction to resolve and reconstruct the various symmetry mismatches at the motor vertex of the phage². With inherent symmetry mismatches reconciled, it was possible fit atomic resolution structures of individual components into their corresponding density, resulting in the first pseudo-atomic structure of a dsDNA packaging motor (not shown).

More recently, we used X-ray crystallography to determine the structure of a pentameric ring of an ATPase from a φ29-like phage, asccφ28⁷; this is the first and only structure of the ring form of a packaging ATPase from any virus (other structures are of catalytically incompetent monomers or individual domains within monomers) and showed that in the absence of DNA the motor is planar (Fig. 1B). Each subunit consists of an N-terminal ASCE ATPase domain and a C-terminal vestigial nuclease domain connected by a smaller lid subdomain that closes over the active to interact extensively with the neighboring subunit. The lid subdomain is thus positioned to coordinate adjacent subunits in response to the binding state of the active site. Further, the active site is nestled between two neighboring subunits: the cis-monomer contributes the conserved Walker A and Walker B nucleotide binding and catalytic motifs while the trans-monomer contributes a conserved lysine and arginine (Fig. 1C). We proposed that the lysine triggers catalysis, stabilizing the ATP transition state, whereas the arginine is involved in nucleotide exchange¹⁹ (see below, Computational advances).

Further, we imaged φ29 particles stalled during packaging via the addition of the non-hydrolyzable γ-S-ATP by cryoEM⁸. Using a series of nested, highly-focused reconstructions, we determined the first and only near-atomic resolution structure of a packaging motor assembled on a capsid (Fig. 1A). This structure showed that the N-terminal ASCE domain (NTD) of the ATPase adopts a helical structure complementary to the dsDNA in the ATP-bound state, in contrast to our planar X-ray structures in the absence of DNA.

Computational advances: Our helical and planar ATPase structures provide structural correlates to the mechanochemical cycle derived from single-molecule experiments. To explore how the motor transitions between states, we did long time-scale molecular dynamics (MD) simulations⁷. Initial MD simulations of the φ29 pentameric ring without DNA predicted that the flexibility of the lid subdomain depends on the nucleotide occupancy; the lid is flexible in the apo-state but rigid when bound to ATP or ADP. MD of ATPase monomers suggested that when ATP binds the lid subdomain rotates to close over the active site; in contrast, in the apo-state the lid remains flexible and extended. For ADP binding, the lid behavior is somewhere in between; the lid closes over the active site but does so less vigorously. We noted that as the lid rotates over the active site in the nucleotide-bound states, it would pull on the neighboring subunit, bringing it closer to itself. Additionally, the region it pulls on is where the trans-acting lysine and arginine are located (Fig. 1C). Hence, ATP binding in one subunit would bring its neighbor closer, and, in doing so, position the trans-acting, catalytic residues into position to facilitate hydrolysis. To further discriminate between ATP- and ADP-binding effects, we extracted two adjacent subunits in the ring, docked ADP in their shared active site, and performed long time-scale MD simulation. This simulation suggested how nucleotide exchange occurs: at the beginning of the simulation a lysine in the Walker A motif of the cis-subunit binds the β-phosphate of ADP and as the simulation proceeds the β-phosphate is transferred from a cis-acting lysine to a trans-acting arginine (R146). Since R146 is closer to the periphery of the active site entrance/exit, we hypothesize that this transfer event initiates the release of ADP and facilitates nucleotide exchange during the dwell.

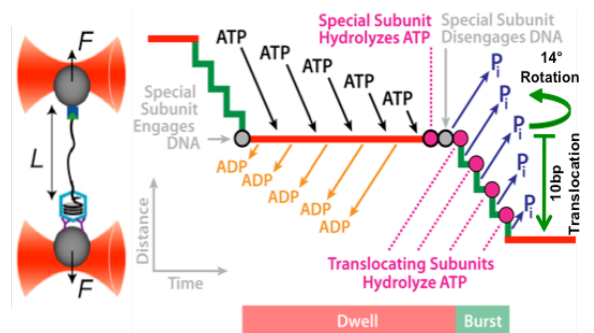


Fig. 2: (Left) Geometry of laser tweezers assay. **(Right)** The previously described φ29 DNA packaging mechanochemical model.

Mechanistic interpretations: The observed helical structure in the ATPase agrees with an emerging trend in cryoEM of ASCE motors²⁰. Structures of these ATPases complexed with their polymeric substrates showed that these structures also adopt a helical arrangement of subunits rather than a planar-ring organization. Based on these structures, a ‘hand-over-hand’ mechanism was proposed for polymer translocation²⁰. In this mechanism, the subunit at the top of the helix hydrolyzes ATP as it releases its polymeric substrate. The next subunit in the helical arrangement then moves up and into the top position previously held by the subunit that just fired, which then moves to the bottom of the helix. As a result of this helical treadmilling by ATPase subunits, the ATPase helix slithers along its polymer substrate in a hand-over-hand, spiral escalator-type mechanism. By induction, φ29 might use a similar hand-over-hand, spiral escalator-type mechanism to propel its dsDNA into the procapsid. Indeed, the experiments described below will help confirm or refute such a model.

While there are many attractive aspects of a hand-over-hand mechanism for viral packaging motors, there are also concerns. Primarily, the dwell-burst behavior in φ29 does not naturally emerge from such a mechanism. Escalators are continuous and do not pause as the last step reaches the top/bottom. Further, we observed the φ29 ATPase in planar configurations, both in the structures of isolated ATPases and in structures of motors assembled on procapsids without DNA. Hence, we proposed a new mechanism for DNA packaging (Fig. 3). The essence of the mechanism is that the motor cycles between extended helical and compressed planar configurations to ratchet DNA into the procapsid. The transition from the helical to planar states drives DNA translocation during the burst phase, while the transition from the planar to the helical state resets the motor during the dwell phase.

Mechanism of force generation. In our model (Fig. 3), ATP binding drives two competing effects. The predominant effect is increased affinity for DNA, resulting in the N-terminal ASCE ATPase domains adopting a helical configuration complementary to the helical phosphate backbone, as observed in our cryoEM structure of stalled particles (Fig. 1A). The competing effect of ATP binding is lid subdomain rotation over the active site, as observed in long time-scale MD simulations. Because the lid subdomain is bound to a neighboring subunit (Fig. 1B), this effect would drive subunits into a co-planar configuration if not for the interaction with the helical DNA. The tension between the two effects is resolved when a subunit hydrolyzes ATP and thus releases its grip on DNA. No longer constrained by its interaction with DNA, the lid subdomain of the adjacent ATP-bound neighbor can now rotate, bringing both subunits into a planar configuration (Fig. 3A-E). Since the ATP-bound subunit(s) maintains grip of DNA, this results in a stepping of the DNA past the hydrolyzing subunit, through the ring and into the procapsid. Thus, resolution of the competing effects of ATP binding provides the basis of force generation and DNA translocation.

Events in the burst phase. A detailed description of the mechanochemical cycle starts when all five subunits are ATP-bound and therefore in the helical configuration (Fig. 3A). The subunit at the top of the helix (S1) hydrolyzes first and releases its grip on DNA,

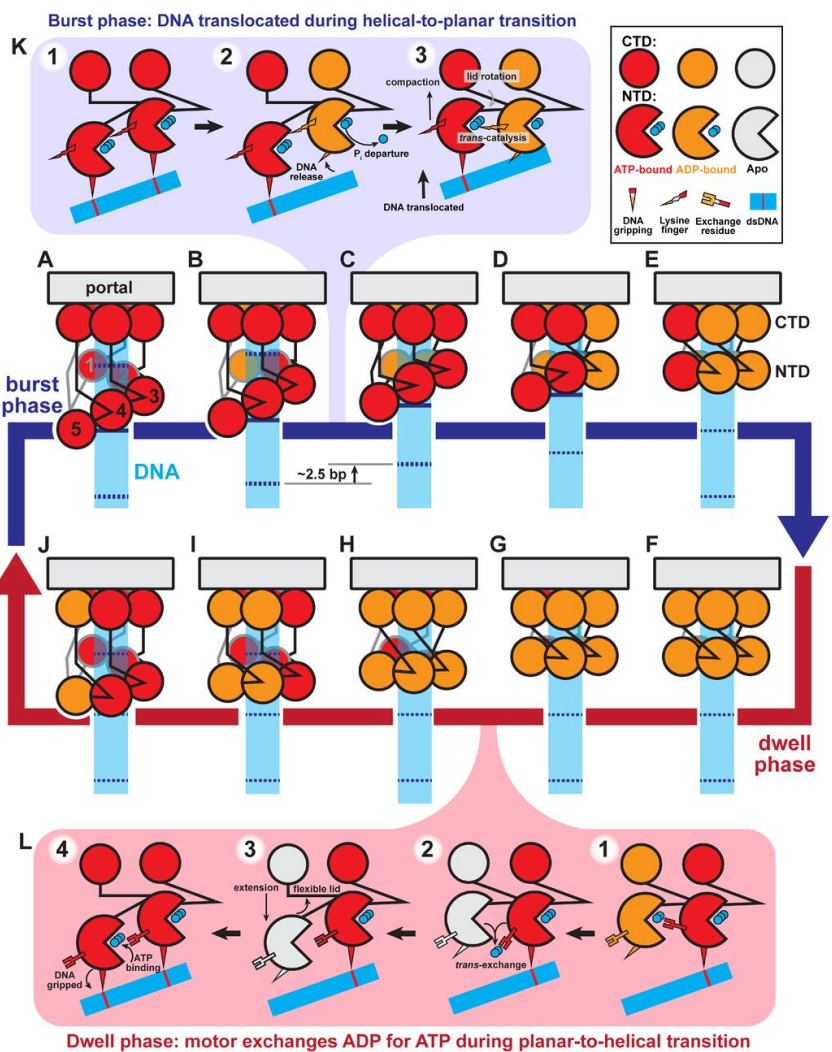


Fig. 3: Schematic of helical-to-planar ratchet model of DNA translocation. During the burst (A-E), ATP-bound subunits (red) sequentially hydrolyze ATP. Hydrolysis in a subunit causes a pair of NTDs to become planar, translocating DNA. At the end of the burst, all subunits are ADP-bound (orange). During the dwell (F-J), ADP is sequentially exchanged for ATP, extending the planar NTD ring back into the helical form. DNA is depicted as a cyan rectangle, and helical-repeat of DNA are dashed lines. K and L are described in the text.

allowing its ATP-bound neighbor (S2) to rotate its lid subdomain and bring both subunits into a planar configuration (transition between **Fig. 3A** and **B**). Since the remaining subunits (S2–S5) have yet to hydrolyze ATP, they continue to grip DNA such that ~2.5 bp of DNA are translocated into the procapsid. Upon co-planar alignment, the transacting lysine finger of the now-ADP-bound subunit is positioned to trigger hydrolysis in the adjacent ATP-bound subunit (**Fig. 1C, 3K**). Hydrolysis at this subunit initiates the next translocation step, as the hydrolyzing subunit releases grip on DNA, and lid subdomain of the ATP-bound adjacent subunit rotates, bringing both subunits into plane and translocating DNA as in the previous step (transition between **Fig. 3B** and **C**). This pattern of hydrolysis at one subunit coordinating force generation of the adjacent subunit permutes around the ring until all N-terminal ATPase domains are in the planar configuration (**Fig. 3C–E**). The result of one complete helical-to-planar transition is translocation of ~10 bp, or one helical turn, of DNA in four sub-steps. Thus, the helical-to-planar transition coordinated by sequential ATP hydrolysis constitutes the burst phase of the mechanochemical cycle.

Events in the dwell phase. Once the motor is in the planar configuration, the final hydrolysis event would not translocate DNA (transition between **Fig. 3E–F**). However, hydrolysis at the final subunit (S5) is needed to release DNA, such that the motor can step back down DNA during the reset. Additionally, single-molecule studies have suggested that the fifth, non-translocating hydrolysis event plays a coordination role^{11,12}. Thus, the final hydrolysis event likely coordinates the initiation of nucleotide exchange (**Fig. 3F**). The final subunit, whose N-terminal domain is now in plane with the N-terminal domain of the subunit that began the translocation burst (S1), donates its trans-acting arginine exchange residue to promote nucleotide exchange in the first subunit (transition between **Fig. 3L; Fig. 1C**). Because DNA was translocated one helical turn, DNA's translational symmetry ensures that the subunit that began the burst (S1) is now positioned to reengage a DNA phosphate one helical turn below its last bound position. This highlights the importance of critical electrostatic contacts every helical turn of DNA observed in SMFS experiments²⁰. After ATP binds at the first subunit, it reengages DNA, locking its N-terminal domain in place. Then its transacting arginine exchange residue promotes nucleotide exchange in the adjacent subunit (S2) (transition between **Fig. 3G–H**).

INNOVATION: Our group has a rich history of innovation and development of novel experimental approaches, analyses, and instrumentation. **Single molecule innovation:** 1) the first viral packaging system adapted to optical tweezers⁵; 2) magnetic tweezers-fluorescence microscopy to test a long-standing 'portal' rotation hypothesis²¹; 3) use of ultrahigh-resolution optical tweezers to resolve motor stepping on the base-pair scale¹¹; 4) Single molecule measurement of DNA rotation by the motor¹³; 5) delineation of DNA-motor contacts using modified DNA and RNA substrates^{9,22}; 6) measurement of symmetry-breaking events that lead to labor division among subunits¹²; and 7) description of how head filling modifies all aspects of the motor mechanochemistry¹³.

The research proposed here expands this innovative trend by pushing the experimental frontiers of single molecule analysis. We will use a combination of high-resolution optical tweezers assays with single molecule imaging of labeled motors to detect changes in motor configurations during packaging. In most other *in vitro* single-molecule assays the motor of interest is largely removed from its biological context to simplify the experiment. Consequently, these assays paint an incomplete picture in that they often lack factors that modulate operation. In contrast, the fully reconstituted φ29 system permits manipulation of every component of the packaging complex, allowing us to investigate the role of regulatory factors¹³. PI Bustamante's laboratory houses one of the first state-of-the-art fluorescence-force hybrid optical traps in the world, with base-pair resolution and single-fluorophore sensitivity²³. This instrument will enable us to correlate conformational dynamics within the φ29 motor complex with motor stepping during DNA translocation, bridging the gap between static structural information and dynamic single-molecule observations (**Aim 2.2** and **2.3**).

Image processing innovation: 1) We were the first group to image functional particles in the process of packaging DNA¹⁴; 2) PI Morais pioneered the type of highly focused reconstructions and symmetry-breaking approaches²⁴ that are now routinely used in image processing of viruses and other macromolecular complexes. 3) We developed software, FOLD-EM, based on the Scale Invariant Feature Transform (SIFT), to detect and characterize conformational changes in macromolecules imaged via cryoEM²⁵.

To extend these efforts, we will employ state-of-the-art image processing approaches to structurally characterize inherently dynamic motor components including: 1) using AI-based image processing algorithms to reconstruct conformational variability; 2) taking advantage of the variance of cryoEM data to identify and reconstruct dynamic regions of macromolecules; and 3) using cryoEM to derive energy landscapes from cryoEM data and using them to order different states as conformational trajectories. Hence, while conformational heterogeneity is often considered a hindrance in cryoEM image processing, we will extract meaningful information about motor dynamics from this aspect of the data.

APPROACH: Hypothesis: The *helical-to-planar model* described above is our primary hypothesis regarding how dsDNA viruses package their genomes. The hand-over-hand model would thus serve as a competing hypothesis²⁰. These two models share common features; both mechanisms invoke adjacent subunits transitioning between co-planar and helical configurations. They differ in the number of transitions necessary to execute a mechanochemical cycle. In our model, all five subunits participate in each cycle, while at the other extreme in the hand-over-hand model only one pair of subunits transitions per cycle. One could also imagine intermediate models where some, but not all, pairs of subunits transition in a single mechanochemical cycle. Hence, we will experimentally test these models of DNA packaging, and generate data necessary to extend/adjust existing models or generate new models for packaging. Our results will illuminate the principles of dsDNA packaging motors as well as the broader class of ASCE ATPase ring motors from which they derive.

Aim 1: Characterize the structure, dynamics, and energy landscape of DNA packaging motors. The defining feature of our proposed helical inchworm mechanism is that pentameric ATPase motors systematically cycle between helical and planar configurations to ratchet the dsDNA genome into the procapsid^{7,8}. While this mechanism explains existing data regarding DNA packaging, it also makes explicit predictions, including the relationship between motor configuration and DNA/nucleotide binding. Hence, **Aim 1.1** will employ now-routine cryoEM single-particle approaches to determine the extent to which helical-to-planar transitions occur over the ring, and how these transitions are coupled to DNA translocation and nucleotide binding. In **Aim 1.2** advanced image processing approaches will be employed to characterize motor dynamics, and to derive energy landscapes from cryoEM data and use them to map conformational trajectories that drive packaging,

Aim 1.1 Test structural predictions of the helical to planar model. Our mechanism predicts that the motor will adopt a helical configuration, driven by ATP-dependent DNA-binding, at the beginning of the burst when all five motor subunits have bound ATP. Sequential ATP hydrolysis and release of the ATP-dependent DNA contact begins at the top of the helix and the ring gradually transitions to a planar configuration during the burst, driving the DNA through the lumen of the ring. This mechanism is largely based on the cryoEM structure of the motor showing that the NTD of the ATPase adopts a helical configuration when ATP is bound (**Fig. 1A**). While this is compelling evidence, it represents only a single endpoint of the mechano-chemical cycle, and thus is not conclusive. Hence, for the first part of this sub-aim, we will image the other endpoint of our proposed mechanism, *i.e.* the end of the burst/beginning of the dwell when all five subunits have ADP bound. Based on our success imaging particles stalled at the end of the dwell via addition of the non-hydrolyzable ATP analog γ-S-ATP, we will use a similar approach to stall the motor in an all-ADP state at the end of the burst. Briefly, we will initiate the packaging reaction as previously described, however, rather than adding an excess of γ-S-ATP, we will flood the system with ADP. Unpackaged DNA will be degraded, again as described previously, before applying the ADP-stalled packaging particles to grids for freezing and subsequent imaging via cryoEM. Reconstructing particles with ADP and DNA bound may be challenging due to the predicted inherent flexibility and dynamics of the packaging motor in this state and the complex symmetry mismatches between the massive C5-symmetric capsid, the relatively tiny ~C12 portal, the 10₁-helical DNA, and the almost surely C1 ATPase. However, we are confident that the nested, highly focused reconstruction approach used for the ATP/DNA-bound structure will allow us to faithfully reconstruct the motor.

While this structure would allow us to determine whether the gross features of the helical-to-planar mechanism are correct, it could not directly confirm the energetic framework of our model, *i.e.* that force generation results from resolving the competing effects of ATP binding via ATP hydrolysis in one of the subunits. Specifically, our model predicts that ATP-dependent DNA binding causes adjacent subunits in the ring to adopt a helical offset guided by the DNA helix. Since the helical configuration depends on DNA binding, in the absence of DNA our model predicts that both ATP and ADP binding would cause lid subdomain rotation, resulting in the planar configuration. Hence, we will determine high resolution cryoEM structures of ATP- and ADP-bound motors assembled on capsids in the absence of DNA. The production and imaging of these particles has been previously described by us^{26,27}; a similar approach will be used for high resolution imaging. Reconstructions of motors in the absence of DNA should be straightforward, with atomic resolution maps readily attainable via standard cryoEM single particle analysis. While these DNA-free structures represent off-pathway particles, they will help determine if the proposed energetic framework of the model is correct.

Aim 1.2: Characterize the dynamics and energy landscape of packaging motors: As with mechanical devices on the macro-scale, understanding molecular motors depends on understanding how different motor components move and interact with respect to each other. Hence, we will use advanced imaging processing approaches to characterize flexible/dynamic regions of motor components and to document structural changes in the motor that accompany packaging. These results will allow us to better understand how changes in

molecular structure and dynamics upon nucleotide binding give rise to the gross quaternary changes that define the helical-to-planar mechanism or give rise to alternate models of DNA translocation.

Aim 1.2.1: To identify mobile, conformationally heterogeneous regions of the motor and characterize the structural changes that drive packaging, we will analyze cryoEM images of particles flash-frozen during DNA packaging. Thus, the full spectrum of conformational states traversed by the motor will be represented in the data. Several groups have recently written software that uses artificial intelligence (AI) to characterize conformational heterogeneity present in cryoEM datasets²⁸. These programs are generally developed by training the AI using conformational ensembles produced by MD simulations. Hence, while we will analyze our data using such programs (such analyses are generally part of the default procedures in modern image processing software), we are cognizant that limitations in MD-derived training sets may restrict the types of conformational heterogeneity that can be detected and reconstructed. Thus, we will also employ image processing approaches wherein information about dynamics comes entirely from the data itself.

Another straightforward approach that we will pursue is to use projections of multiple models along with maximum likelihood approaches to classify particles not only according to viewing direction but also according to conformation. While previous knowledge of different structural models is helpful, it is not always necessary. Often, adding random noise to two or more otherwise identical structural models provides sufficient information to begin the process of conformational sorting. Bootstrapping over several iterative cycles often leads to convergence of the process, allowing the resolution of distinct conformational states of a complex^{29,30}.

Further, we will employ a related approach utilizing multibody refinement to analyze dynamic macromolecules. In this approach, the experimentally obtained 2D image of a complex/macromolecule is treated as a sum of the projections of distinct macromolecules within the complex and/or individual domains within subunits. Hence, a cryoEM image of a two-domain protein might be considered as a sum of the projections of two domains, A and B. If there are multiple conformations characterized by different relative orientations of A and B, these can be detected and possibly reconstructed by matching experimental images to projections of different combinations of relative orientations of A and B. This approach is also already implemented in most modern cryoEM image processing software suites. Of course, this approach can also inform and improve multi-model refinement approaches if distinct conformers are identified. A more mathematically rigorous application of this idea has recently been implemented in CryoSPARC²⁹, wherein a version of principle component analysis is used to generate a continuum of conformers, projections of which can then be used to simultaneously classify particles via both viewing direction and conformation³¹. While not conclusive, observing similar results from different implementations of similar ideas can provide confidence that the observed conformations represent the molecular ensemble rather than an artifact of a particular algorithm.

Aim 1.2.2. To further characterize motor dynamics, we will estimate the more subtle conformational variation present in cryoEM images by examining the statistical variance within the 2D experimental images of a dataset or between multiple, independent 3D reconstructions derived from a single data set^{32,33}. Typically, in cryoEM image processing, common views of a particle are averaged together to produce class averages representing that view. Different 2D class averages representing different views of the particle are then assembled to produce a 3D volume. For back projection-based 3D reconstruction approaches, the average density value at each pixel position in individual image belonging to a class is back-projected during 3D reconstruction.

Similarly, in Fourier-based methods, the average value at each pixel position in a class average is fed into the summation/integral of the Fourier transform. Even though explicit class averages are not always used in the 3D reconstruction procedures, equivalent pixels from images of the same view are nonetheless averaged during reconstruction of the 3D volume. To characterize conformational heterogeneity/molecular flexibility, we will instead generate 3D maps *from the standard deviations of equivalent pixels* in images of particles presenting the same view rather than the average value as is customary. Such ‘maps’ display the heterogeneity of the particle as the variance plotted at each voxel of the reconstructed 3D volume. This variance can be used to locate conformational variability, thus revealing regions of the motor that move during translocation. This approach is intended to locate dynamic regions of the motor. However, in the best-case scenario, regions with high variance can be mapped back on the 2D experimental images of each particle, and the images sub-classified based on the pixels in these regions. Sub-classes of particles from different motor conformations could then be used to generate snapshots of distinct intermediates. Hence, this approach will inform motor dynamics by revealing which parts of the motor are in motion during packaging, and could possibly facilitate classifying and reconstructing distinct packaging intermediates.

Aim 1.2.3. We will use large data sets ($> 10^{6\text{th}}$ or $10^{7\text{th}}$ particles) of the packaging ATPase ring motor to determine the energetic landscape of motor ring ensembles and to map the conformational trajectories the

motor follows upon nucleotide binding. Different conformations of projections of particles viewed from the same direction reside on manifolds in multi-dimensional classification space. Due to the relationship between the occupancy of a particular state and free energy described by the Boltzmann equation, the number of particles at each point on this subspace is thus related to the energy landscape of the particle. Highly populated conformational states correspond to deep energy wells, and any extended ‘canyons’ map the most likely trajectories that macromolecules traverse to change conformations^{34,35}. Distinct energy landscapes can be determined for apo-and ligand-bound states. By comparing these landscapes, it is possible to identify conformational pathways that macromolecules follow to bind their ligands. Further analysis of such pathways, together with MD analysis, shows the extent to which a binding event follows an ensemble population shift vs an induced fit model, as has been shown for the Ca++ binding receptor RyR1³⁴. Of course, such an analysis requires data sets with large numbers of particles to see sparsely populated states, and signal regarding conformationally variant regions can be masked by signal from static regions. Hence, it is unlikely this approach could be used to analyze DNA packaging particles due to the complexity of the system, the small mass of motor relative to the capsid and DNA substrate, and the challenges associated with collecting sufficient numbers of images of packaging particles. However, evaluating nucleotide binding using the isolated pentameric ATPase ring from the φ 29 relative ascc φ 28 is well suited to this approach. Indeed, large data sets of this sample are readily accessible, and we have already determined high resolution structures of apo-, ATP-, and ADP-bound structures to better than 3 Å resolution. While the resulting information would not show the helical-to-planar transition due to the absence of DNA, it will illuminate nucleotide binding and release pathways, including loose- and tight-binding ATP binding events by motor subunits, showing how binding events in individual subunits might give rise to the quaternary rearrangements required by the helical-to-planar or other packaging mechanisms.

In an exciting recent development, we have found that these isolated motor rings can engage DNA. This is the first example of any DNA packaging ring motor that can translocate DNA without being assembled on a procapsid. This result opens the possibility of expanding our analysis of the motors energetic landscape and resulting molecular trajectories to include DNA binding along with nucleotide binding. Indeed, we have recently determined the structure of the pentamer ascc φ 28 ring motor engaged with DNA and stalled via addition of γ -S-ATP. The resulting structure shows a helical arrangement of ATPase subunits similar to that seen in motors assembled on procapsids. This result indicates that isolated ring motors interact with DNA similarly to motors assembled on procapsids, and opens the door for evaluating how both DNA and nucleotide binding affect energy landscapes and conformational trajectories of an ASCE ring motor. While the resulting information would not show the helical-to-planar transition due to the absence of DNA, it will illuminate nucleotide binding and release pathways, including loose- and tight-binding ATP binding events by motor subunits.

Preliminary results: We have recently been able to stabilize and purify φ 29 particles representing ADP-bound DNA packaging intermediates by adjusting buffer conditions and shortening the time taken to prepare material for microscopy, thus overcoming the most significant previous barrier to imaging these intermediates. The packaged DNA remains protected from nuclease treatment for hours, ensuring that we can freeze and image sufficient numbers of particles for high-resolution image reconstruction. As discussed above, once imaged, we will utilize nested, highly focused classification and image processing strategies used to reconstruct the helical endpoint-state of the motor at the end of the dwell. We have already determined DNA-free structures of isolated pentameric ATPase motors from the φ 29-relative ascc φ 28 in the absence of procapsids to better than ~3 Å for ATP and ADP-bound structures, and to ~3.4 Å resolution for isolated rings engaged with DNA and bound to γ -S-ATP. Both the isolated ATP- and ADP-bound ring motors in the absence of DNA assume the planar configuration and have nearly perfect C5 symmetry, whereas the motor bound to DNA adopts a helical configuration similar to that seen for our reconstruction of particles stalled with γ -S-ATP.

Expected results and potential pitfalls. Based on our proposed mechanism, we expect to observe the ADP-bound motor in situ in a planar configuration for sub-Aim 1.1. Strategies for overcoming image processing barriers were discussed above. While there may be additional problems imaging φ 29 motors assembled on procapsids, we could image isolated ascc φ 28 ring motors engaged with DNA and bound to ADP similar to the structures described in preliminary results for isolated γ -S-ATP-bound motors engaged with DNA; the absence of DNA and shared C5 symmetry of the capsid and ATPase greatly simplifies the problem on isolated ring motors. Of course, it is possible that our structural predictions are incorrect, and the ADP-bound motor has a non-planar configuration. However, observing that the ADP-bound motor is in a non-planar configuration would be as valuable as the predicted result since it would allow us to revise our mechanism accordingly. For example, if the motor remains helical, this result would support the hand-over-hand mechanism. Similarly, if

only a subset of subunits were arranged in a planar conformation with the others adopting a helical offset, this result would require us to adjust or completely rethink our proposed model.

While it is inherently difficult to extract molecular dynamics information from cryoEM images, there is increasing precedence in the literature that doing so is feasible³⁶⁻³⁸. Thus, we are confident that sub-Aim 1.2 will generate useful information. Firstly, the number of different approaches proposed above increases the likelihood that meaningful dynamic information can be obtained; indeed, if different strategies yield similar results this increases our confidence in their validity. Second, although it is unlikely that all intermediates can be identified and reconstructed, the proposed analysis of statistical variance in the data will reveal which regions of the motor are mobile; this is highly valuable in interpreting and refining our mechanistic model. Finally, as discussed above, preliminary results on the ascc φ 28 pentameric motor ring suggest that they are well suited for generating energetic landscapes associated with nucleotide binding and product release.

Aim 2: Single-molecule studies of ring motor mechanism – Among the advanced methods we have developed to the study of the φ 29 DNA packaging model system, single-molecule approaches have been greatly informative in allowing us to describe the dynamics, coordination, and communication of this complex machine. Indeed, single molecule results created essential powerful constraints in proposing our packaging model. In this aim, we will extend our development and application of cutting-edge single molecule techniques to characterize both the force-generation and the extensive network of communication required to maintain the high degree of coordination necessary for motor function. *This work will evaluate mechanistic predictions of our model as well as establish a foundational level of understanding of ring-motor mechanisms that could serve as a touchpoint for the ASCE motor field.*

Aim 2.1. Dissect how key residues participate in critical functions during DNA translocation: Armed with the detailed insights we have gained over the past several years, we will perform a series of single-molecule experiments to dissect the roles key elements play during the mechanochemical cycle of the φ 29 motor. In this sub-aim we focus on two key features of this motor: 1) the load bearing contacts between the motor and DNA substrate, and 2) the communication circuits within and between ATPase subunits.

Aim 2.1.1 Interrogate DNA gripping by channel residues. Like other DNA translocases and helicases^{39,40}, the φ 29 motor establishes electrostatic contacts with its substrate that are believed to drive their interactions along their polymeric tracks. Our single-molecule studies showed that during the dwell the motor establishes electrostatic contacts with a pair of adjacent backbone phosphates on the 5'-3' DNA strand every 10 bp²². Our recent structural studies show that the channel through which the translocating DNA moves during packaging is lined with multiple charged residues that might interact with the DNA^{7,8}. Implicit in our mechanism is that some of these residues hold the DNA in place while the motor exchanges ADP for ATP during the dwell; others form the contacts that drive the planar ring into a helical conformation. Here we test which residues form load bearing contacts and/or how these interactions between the motor and the DNA coordinate and regulate the mechanochemical cycle. These include K56, S99, N126, S127, N128, and Y129 in the N-terminal ATPase domain and K294, R327, K328, and R330 in the C-terminal domain; other residues lining the lumen that might be repositioned during the dwell and burst will be targeted as well, including R122 and K124³⁸.

Alanine substitution, charge inversion, and side-chain-length-altering mutations will be made for all molecule assays. All mutants, even those that no longer show detectable packaging in bulk, will be screened for activity in the laser tweezers as our experience has demonstrated that even mutations with a severe phenotype in bulk can still support measurable activity in single molecule¹⁹. Force-clamp experiments, which measure the stall force of the motor⁵, will be conducted at low- and high-DNA filling and compared to Wt to assess altered force generating capacity. We will also measure alterations to dwell duration, burst duration, slip frequency, and tether failure under low external load. Increased dwell time of mutants relative to Wt indicates altered DNA binding during non-translocating nucleotide cycling and/or slower nucleotide exchange. Alternatively, increased burst time suggests alteration of coordinated hydrolysis mediated by DNA contacting residues²² or dysregulation of DNA release upon ATP hydrolysis.

Mutants displaying an increased slip frequency will be further examined using *high-resolution* tweezers to determine when during the dwell-burst cycle the motor contact tends to fail. Increased slipping by mutants during the dwell implies failure to establish contacts with the phosphate backbone upon ATP binding. Increased slipping during the DNA translocating burst implies a disruption of the DNA-release/translocation steps. Increased slipping in mutants in the C-terminal domain would support a proposed role for DNA contacts in the always planar C-terminal ring^{8,18}. In particular, such slipping during the dwell suggests a role for load-bearing contacts in the C-terminal plane of the motor that help it maintain its grip on DNA as the N-terminal domain is cycling nucleotide and rebinding DNA.

Preliminary Results: The Y129I mutant has been produced and shown to support DNA packaging. Interestingly, this mutant yields partially-filled heads in bulk experiments, suggesting slower translocation and/or reduced capability for force generation at high filling as resistive forces increase. The single-molecule phenotype shows that these rings are prone to slips and some translocation events are smaller than 10 bp (**Fig. 4**). We are currently studying this mutant in more detail using higher external forces to test its ability to exert force. More conservative substitutions, such as Y129F and Y129W, are currently in preparation.

Preliminary single-molecule assessment of motors with a K124A substitution are slower and slip more frequently than wild-type in low ATP conditions, when the motor requires more time to load ATP (not shown). These observations suggest that K124 does not establish a critical DNA contact during the burst, but rather has a load-bearing role during the dwell phase that prevents DNA slippage during nucleotide cycling.

By comparison, mixtures of the packaging-defective mutant R122A and Wt result in heteromeric motors, where some subunits in the ring have the mutations and others are wildtype. These heteromeric motors support packaging and exhibit a variety of different behaviors depending on the percentage of mutant in the mixture. In general, very long dwell times are observed for these motors (**Fig. 4**), suggesting a role for R122 in coordinating nucleotide exchange through its DNA interaction.

Based on these and other mixing experiments (see below), we have shown that we are able to discriminate between subtle phenotypes that result from the randomized assortment of mutant and Wt ATPase subunits in the motor ring. Using mixtures of a mutant with a severe phenotype and Wt, we can probe the function of residues otherwise intolerant to substitution. For motors with >1 mutant subunit, we have shown that increasing the number of mutants in a ring can create distinguishable phenotypes that become increasingly severe¹⁹. Thus, a seemingly confounding variable can become a rich source of information revealing progressive phenotypes that emerge with increasing mutant:Wt ratios. Further, previous optical tweezer experiments show that the motor occasionally changes registry with respect to the DNA, eg. which subunit is in which position around the asymmetric motor^{12,22}. By correlating changes in registry to changes in packaging phenotype we can infer the effect of position in the heteromeric, i.e. whether a mutant is tolerated at any or only at a single position. Hence, although this approach yields complex data sets, it enables us to characterize positional tolerance of a wide range of mutant motors.

Finally, we have determined that our preliminary assessment regarding which ATPase residues are critical for DNA contact and force generation is overly simplistic and depends on more than observed charged side-chains interacting with the DNA phosphate backbone; *structural observations require experimental validation*. Specifically, we have shown that residue K56, observed by cryoEM to interact with DNA³, is not essential for *in vitro* DNA translocation, arguing against this residue's role as a load bearing motor contact. Rather, particles packaged with K56A mutant ATPase are unstable after filling, suggesting that the observed DNA contacts do not participate in force generation/translocation, but rather stabilizing DNA at the end of packaging. Preliminary optical tweezers experiments on this mutant and an intermediate phenotype mutant, K56R, are underway.

Aim 2.1.2 Dissect the mechanism of communication and coordination of the motor: We have shown that events during φ29 DNA packaging are highly coordinated¹³. However, we know very little regarding the molecular basis for the coordination needed to maintain the order and timing of events. In this sub-aim, we will examine the mechanism of intersubunit communication and coordination by mutating conserved trans-acting elements in the φ29 motor that we predict are responsible for intersubunit coordination.

Preliminary results: To investigate the role of the trans-acting nucleotide exchange factor, R146^{7,19}, we have collected single-molecule data on heteromeric motors by mixing Wt and R146K or R146A mutants (**Fig. 5**) and on F145I homomeric ring motors¹⁹. Briefly, since R146-mutant subunits do not support packaging as homomeric rings, they were mixed with Wt ATPase to produce motors with different numbers of mutant subunits. Mixing of Wt and mutant ATPase results in a heterogeneous population of motors with variable numbers of mutants in various positions around the ring. Although the overall packaging rate of such a mixture of R146K and Wt is variable, there is nonetheless an overall decrease in packaging rate as we increase the ratio of mutant to Wt (**Fig. 5a, 5c**). In contrast, Wt mixing experiments with the more drastic R146A substitution

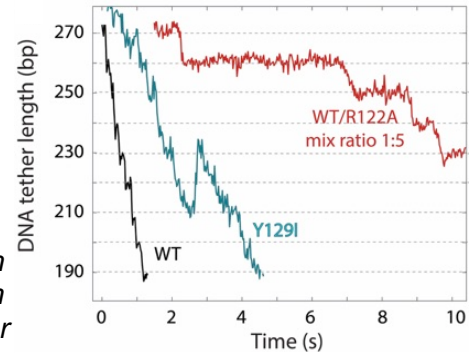


Fig. 4. Probing motor-DNA contacts. Detail of traces from two mutants predicted to interact with DNA: homomeric Y129I rings and hybrid WT/R122A rings from a mixture containing 83% mutant subunits. Y129I traces are rich in slippage events, implying perturbation of steric contacts during the burst, while WT/R122A traces have protracted dwells, suggesting a disruption in the regulatory contacts with the DNA phosphate backbone during nucleotide cycling.

resulted in a sample with only two populations (Fig. 5b, 5d): a Wt-like population and a uniformly slower population. Our data argues that R146K/Wt heteromeric rings can tolerate several mutant subunits before the packaging activity is completely abrogated; possibly lysine can function similarly to arginine. In contrast, data for R146A/Wt heteromeric rings suggest that only one mutant subunit can be tolerated, in this case likely due to the very different chemical properties of alanine. Hence, although we cannot be certain of the number and position of the mutant subunits in each ring, we have demonstrated that it is nonetheless possible to infer valuable information using our mixing strategy (Fig. 5).

As noted above, since nucleotide exchange and coordinated catalysis are segregated between the dwell and burst phases, it should be possible to identify which of these processes are affected by substitutions by

determining which phase of the cycle is altered. For example, even though R146A/Wt heteromeric motors are slower, the size of the burst remained ~10bp (Fig. 5e), indicating that four subunits are still powering translocation, and therefore must retain catalytic activity during the burst. Because there are five subunits, this observation is consistent with our previous inference that packaging rings can tolerate a single R146A mutant subunit. Indeed, we showed previously in nucleotide poisoning experiments (*i.e.* the addition of γ -S-ATP or AMP-PNP) that Wt motors can still function with a temporarily inactivated subunit¹². The most likely explanation is that the one R146A subunit tolerated in the ring is the non-translocating subunit, mimicking a γ -S-ATP bound subunit. Additionally, the dwell times of R146A/Wt heteromeric rings are lengthened 10-fold and are exponentially distributed (Fig. 5f), indicating that a single kinetic event has become rate-limiting. To determine the role of R146 in the context of regulation of the mechano-chemical cycle we are currently performing additional experiments to examine how the rate of each step is affected by these substitutions.

Proposed experiments: We will conduct an extensive series of single-molecule experiments similar to those described above to explore the communication network that regulates the complex mechanochemical cycle of the $\varphi 29$ motor. We will thus study another putative trans-acting residue, the K105 lysine shown by our structural studies to be in close proximity to the gamma-phosphate of the ATP^{8,17}. Early bulk poisoning trials of Wt subunits mixed with alanine- or arginine-substitution mutants (K105A and K105R) suggest that these mutants have a poisoning phenotype similar to mutation of the trans-acting R146, thus implying a trans-acting role for K105. Examination of the dwell/burst behavior of mutant-containing rings in optical tweezers will determine which coordination step(s) is/are affected. As we investigate additional mutants informed by our structural studies, we will focus on mutation of residues that lie on both sides of the subunit interface to modulate packaging thus gaining an understanding of communication within the ring.

Aim 2.2 Characterize DNA rotation during DNA packaging. We previously demonstrated that DNA rotates along its long axis during translocation¹³. Under low filling conditions, we measure a rate of DNA axial rotation of ~1.4° per base pair packaged (*i.e.* ~14° per 10bp burst). We hypothesize that DNA rotation occurs to realign the DNA with the ~5-fold symmetric motor; although B-form DNA is often described as having 10₁ symmetry, its periodicity is actually ~10.4bp per helical turn. As a result, translocating one period of DNA is equivalent to rotating it only 346 rather than 360 degrees; hence, the DNA must rotate another 14° such that it is properly realigned with the motor at the end of a burst. Further, as the head fills, the rate of DNA rotation increases to ~50° per 10bp burst, correlating with the decrease in mean burst size from 10 to 9 bps, and thus requiring greater axial rotation to realign the motor with the translocating DNA substrate. A full discussion of this experiment and its interpretation can be found here in Liu *et al.*¹³

Characterizing the nature of DNA rotation and how the magnitude of rotation changes with increased head filling provides us with an opportunity to determine how translocating ATPase motors maintain registry with their polymer substrates. Since this is a general problem that all polymer translocating ring ATPases must

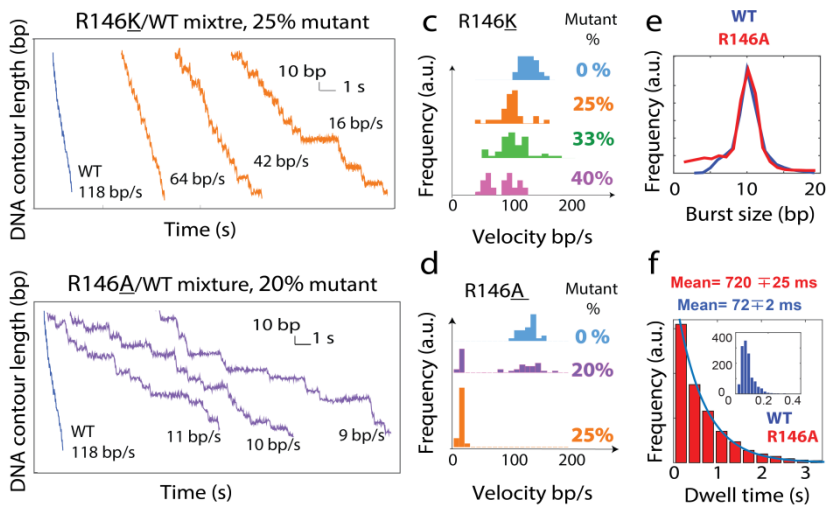


Fig. 5. Arginine finger heteromeric mutant rings. Sample packaging trajectories of a) a 3:1 WT to R146K and b) a 4:1 WT to R146A mixing ratio. WT trace in blue for reference. c) Velocity distribution for 3:1, 2:1, and 3:2 WT to R146K and d) 4:1 and 3:1 WT to R146A mixing ratios. e) Burst size is unaffected by R146A, but dwell time f) is dramatically extended. WT measurements are in blue.

overcome, these experiments will inform similar studies of other ASCE ring ATPases. To experimentally characterize DNA rotation, we begin by considering the two possibilities that define the boundaries of the experiment in φ 29. In one possibility, DNA rotation occurs incrementally during translocation, for example with a rotation of $\sim 3.5^\circ$ accompanying each 2.5bp motor substep. At the other extreme, the entire 14° DNA rotation occurs entirely at the end of each 10bp translocating burst.

Proposed experiments: To evaluate when DNA rotation occurs relative to motor stepping, we will adapt our previous experimental setup¹³ (**Fig. 6**) to the newly

developed combined fluorescence optical tweezers (“fleezers”) instrument. In this altered setup (**Fig. 7**), an engineered 10bp DNA hairpin (3.4nm in length) will be fluorescently labelled and positioned 2kbp from the motor and on the near side of a single-stranded DNA nick that will permit axial rotation of the DNA. As the DNA rotates, the hairpin spins in a direction perpendicular to DNA translocation. By observing the fluorescent probe on the DNA hairpin, we can monitor rotation using polarized excitation and/or polarized emission detection to correlate DNA rotation with DNA translation. One of the most critical considerations for attempting this experiment is calculation of the temporal resolution the experiment can support. The springlike nature of DNA significantly influences our consideration of “reporter” size since flexibility of the DNA tether may dampen the signal from the rotating probe. Likewise, the hydrodynamic drag of the “reporter” attached to the DNA must be low enough to prevent decoupling reporter rotation from DNA rotation. We have calculated the corner frequency (γ_{corner}), which defines the temporal sensitivity of our rotation-reporting experiment as follows:

$$\mathcal{W}_{corner} = \frac{C/L}{\gamma_{rot}} \text{ where } C = \text{torsional rigidity for DNA} = 450 \text{ pN} \cdot \text{nm}^2; L = \text{length of the tether DNA} = 2 \text{ kbp} = 680 \text{ nm}; \text{ and } \gamma_{rot} = \text{drag coefficient} = 14\pi\eta r^3. \text{ Solving for } \mathcal{W}_{corner} = \frac{450 \text{ pN} \cdot \text{nm}^2 / 680 \text{ nm}}{14\pi \cdot 8.9 \times 10^{-10} \frac{\text{pN} \cdot \text{sec}}{\text{nm}^2} \cdot (3.4 \text{ nm})^3} = 4.3 \times 10^5 \text{ sec}^{-1}$$

which relates to the corner frequency by $\mathcal{W}_{corner} = 2\pi\gamma_{corner}$. Thus, the highest frequency with which the rotational position of the hairpin probe can be reported is $\gamma_{corner} = 6.8 \times 10^4 \text{ sec}^{-1}$. This is more than sufficient to report the coupling of DNA rotation to high-resolution motor stepping; our highest observed packaging velocity (20msec/burst) and rotation rate ($\sim 50^\circ/\text{burst}$) yields a rotation velocity is $\sim 7 \text{ Hz}$ ¹³.

Expected results and possible problems

Given the technical difficulty of this experiment, we will first return to the low-resolution “rotor bead” reporting experiment we have used previously¹³ but now adapted to the fleezers. Even though the size of the reporter bead, with its high drag coefficient, precludes the strict correlation between rotation and translocation we seek, it will enable us to break this challenging experiment into pieces that can be revised and refined individually. We will then begin to reduce the size of the reporter, (ex. replacing the rotor bead with eGFP to trouble-shoot the fluorescence polarization conditions) before moving to the higher resolution, labelled DNA hairpin strategy.

Aim 2.3: Correlate changes in motor conformation with DNA translocation: Complementary to the structural analyses of mechanochemical intermediates described in Aim 1, we will use the fleezers to follow changes in motor conformation *in real time* during packaging. Our proposed helix-to-planar mechanism predicts that the N-terminal domains (NTDs) of ATPase subunits move up and down relative to the direction of packaging as the motor transitions between helical and planar configurations. We will attach a FRET donor to the N-terminus of an ATPase subunit and FRET-acceptor probes to a relatively stationary anchor point on the motor, such as the pRNA ring or the portal²¹ (**Fig. 7**), allowing us to monitor NTD movement via changes in FRET signal. To correlate FRET-observed NTD movement to DNA translocation, the dye labelled particles will be tethered between two beads in the fleezers and simultaneously record the shortening of the DNA tether and any FRET changes that occur during packaging. Based on the structure of the motor, we have designed a number of donor-acceptor labelling sites such that the expected distances between them is $\sim 5 \text{ \AA}$ for the planar state of the motor (close to R_0 for the Cy3-Cy5 FRET pair, thus producing maximal signal) and $\sim 40 \text{ \AA}$ for the maximally extended helical state (within a universally accepted distance for FRET-based measurements).

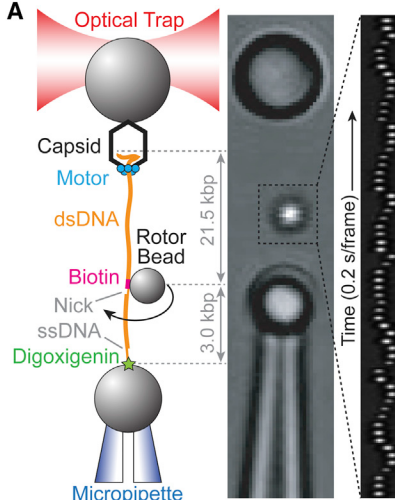


Fig. 6. Experimental geometry of the rotation assay from Liu et al. The packaging complex is tethered between two beads. Biotin-streptavidin linkages torsionally couple the rotor bead to the optically trapped bead via dsDNA. A nick and a ssDNA region ensure that the rotor bead is torsionally decoupled from the micropipette-bound bead. Middle view is a micrograph of the experimental geometry. Right view is a kymograph of the rotor bead position during packaging, displayed at 5 Hz.

Preliminary results: Combined single molecule force-distance and imaging measurement⁴¹ are not yet routine. We have constructed our own freezers setup and used it to study complex motor dynamics.

The chemical labelling of the components needed for these studies has been developed and tested. We have replaced the two wild-type cysteines in the ATPase with serines and then created a new labelling site by replacing serine 4 of the ATPase with cysteine. These S4C mutants label efficiently, and labeled protein retains full activity in the *in vitro* DNA packaging system (not shown). Similarly, we have engineered cysteine labelling sites in the “paper clip” region on the portal, gp10 (residues 168, 170, 189, or 190) which are close to the ATPase ring; all of these connector mutants label efficiently and with specificity, and have full packaging activity²¹. We are in the process of making the other necessary components for the freezers experiments, including DNA handles required to position the packaging complex far enough away from the capsid-bound beads to allow interrogation of the optical probes.

Expected results and possible problems. There are two potential complications to the freezers experiment that we have already taken into consideration. One is the complex symmetry of the motor components. Since we desire a labelled ATPase ring with a single donor probe, we will mix labelled and unlabelled ATPase in ratios that favor a single labelled subunit. The labelled state of individual packaging complexes will be confirmed in the freezers using stepwise probe bleaching. With the acceptor labelling site, we will label all 12 of the portal subunits (alternatively we will label all five pRNAs); multiple acceptor probes forming a ring are ideal as they are able to report FRET interaction with any of the five ATPase subunits, with the change in FRET intensity representing the average signal change between the single donor and multiple acceptor probes. Importantly, changes in this average value will accurately report the change in distance from the single donor probe on the ATPase NTD and the plane of labelled acceptor labelling sites.

The asymmetric nature of our proposed packaging mechanism creates the condition where the change in FRET signal would differ depending on the ring position of the donor-labelled ATPase NTD. For example, based on our model in Fig. 3, FRET donor label on S1 is predicted to not move relative to the acceptor plane, but label on S5 will result in the greatest change in FRET signal distributed across the four mechanical stepping events (Fig. 8). We turn this complication into an advantage since within a data set we would expect to see different FRET “stepping” behaviors for each of the five possible positions of the donor label. This can vary from complex to complex or *within a single complex if the motor is forced to change registry if a burst is incomplete*. The latter can be exploited by forcing the motor to occasionally change which subunit occupies the top position of the NTD helix. From our earlier single molecule studies on motor operation under stressed conditions (ex. operating at [ATP] well below the ATPase Km)^{12,19,22}, the motor occasionally initiates a burst before it is fully loaded with ATP, resulting in bursts of 2.5, 5, or 7.5 bp. Since the subsequent bursts are typically 10bp, these motors have changed registry in order to take a full 10bp burst after an interruption. Thus, we can vary the relative identity of the single donor-labelled ATPase in the ring simply by packaging at low [ATP], allowing us to detect the correlated change in FRET signal for all five ATPase positions by repeatedly changing the motor registry during a single experiment as we have before. We point out here that our group has now extensive experience in the co-temporal measurement of high-resolution optical tweezers and single molecule fluorescence detection²³. Our experiments show that the temporal relationships between the two signals makes it possible to establish causal relationships between the two phenomena being monitored, in this case DNA translocation and conformational change of the motor during its successive power strokes.

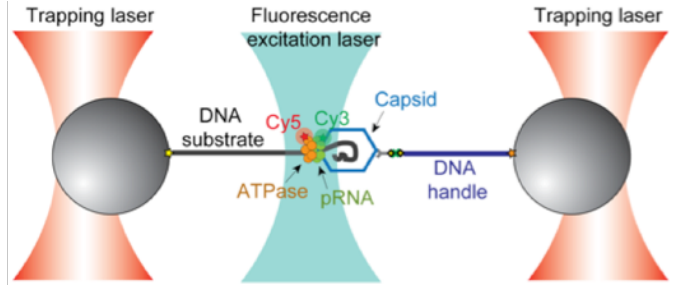


Fig. 7: A single-molecule fluorescence-force assay for studying DNA packaging by the φ 29 motor: example experimental geometry. The FRET donor and acceptor, Cy3 and Cy5, are labeled to the pRNA and the gp16 ATPase, respectively. The capsid is bound to biotinylated antibodies against the capsid protein that are linked to a dsDNA handle for bead attachment.

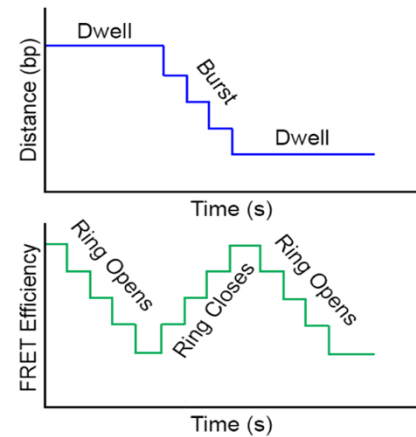


Fig. 8. Schematic of a possible result of the ‘fleezers’ experiment. The simultaneous measurement of DNA translocation (top) and FRET signal (bottom) will show if and how the helical-to-planar occurs during DNA packaging. This example considers donor label on subunit 5 from Fig. 3 which will report all four substeps.